

## Nuclear “pasta” phase within density dependent hadronic models

S. S. Avancini,<sup>1</sup> L. Brito,<sup>2</sup> J. R. Marinelli,<sup>1</sup> D. P. Menezes,<sup>1</sup> M. M. W. de Moraes,<sup>1</sup> C. Providência,<sup>2</sup> and A. M. Santos<sup>2</sup>

<sup>1</sup>*Depto de Física, CFM, Universidade Federal de Santa Catarina Florianópolis, SC-CP. 476, CEP 88.040-900, Brazil*

<sup>2</sup>*Centro de Física Computacional, Department of Physics, University of Coimbra, P-3004-516, Coimbra, Portugal*

(Received 5 December 2008; published 18 March 2009)

In the present paper, we investigate the onset of the “pasta” phase with different parametrizations of the density dependent hadronic model and compare the results with one of the usual parametrizations of the nonlinear Walecka model. The influence of the scalar-isovector virtual  $\delta$  meson is shown. At zero temperature, two different methods are used, one based on coexistent phases and the other on the Thomas-Fermi approximation. At finite temperature, only the coexistence phases method is used. *npe* matter with fixed proton fractions and in  $\beta$  equilibrium are studied. We compare our results with restrictions imposed on the values of the density and pressure at the inner edge of the crust, obtained from observations of the Vela pulsar and recent isospin diffusion data from heavy-ion reactions, and with predictions from spinodal calculations.

DOI: [10.1103/PhysRevC.79.035804](https://doi.org/10.1103/PhysRevC.79.035804)

PACS number(s): 21.65.-f, 24.10.Jv, 26.60.-c, 95.30.Tg

### I. INTRODUCTION

“Frustration” is a phenomenon characterized by the existence of more than one low-energy configuration. The “pasta” phase is a frustrated system [1–3]. At densities of the order of  $0.006\text{--}0.1\text{ fm}^{-3}$  [4] in neutral nuclear matter and  $0.04\text{--}0.065\text{ fm}^{-3}$  [5] in  $\beta$ -equilibrium stellar matter, a competition between the strong and the electromagnetic interactions takes place leading to a frustrated system. The basic shapes of these complex structures were first named [1] after well-known types of cheese and pasta: droplets (bubbles = Swiss cheese), rods = spaghetti (tubes = penne) and slabs (lasagna) for three, two, and one dimensions, respectively. A droplet (bubble) and a rod (tube) have densities larger (smaller) than their surroundings and are normally defined within a Wigner-Seitz cell. The pasta phase is the ground state configuration if its free energy per particle is lower than that corresponding to the homogeneous phase at the same density. The pasta phase is expected to exist somewhere between a solid and a liquid phase, more like a liquid crystal [6]. Its mechanical and thermal properties are likely to depend on its shape, but that study still remains to be done.

These pasta shapes at subnuclear densities are expected to exist both in the crust of neutron stars (zero temperature, very low proton fraction, matter in  $\beta$  equilibrium) and in supernova (finite temperature, proton fraction around 0.3). In neutron stars, the pasta phase coexists with a neutron gas; in supernova, there is no neutron gas or it is very low in density [7].

In a recent work [4], we studied the existence of the pasta phase at zero and finite temperature within three different parametrizations of the relativistic nonlinear Walecka model (NLWM) [8], namely, NL3 [9], TM1 [10], and GM3 [11], the last one generally used in the studies of stellar matter. At zero temperature, two different methods were used: the coexisting phases (CP) and the Thomas-Fermi (TF) approximation. We checked that while the final equations of state (EOSs) obtained with the different methods do not vary much, the internal structures vary considerably. The TF approximation was performed to test the much simpler CP calculation, and we have seen that the success of the CP calculation depends

on the parametrization of the surface energy for very small proton fractions and close to the transition densities. At finite temperature, only the CP method was used and compared with predictions from spinodal calculations. The pasta phase shrinks with the increase of the temperature, and we have found that homogeneous matter can be the preferential phase also at very low densities depending on the temperature and the proton fraction. If  $\beta$  equilibrium is imposed, the pasta phase does not appear in a CP calculation. This indicates the necessity of using a good parametrization for the surface energy which is temperature, proton fraction, and geometry dependent, as also stressed in Refs. [12,13].

The authors of Ref. [14] related the fraction of the moment of inertia contained in the crust of the Vela pulsar with the mass and radius of the neutron star and the pressure and density at the crust-core interface. From a realistic EOS, they obtained an expected range of values for the pressure at the inner edge of the crust and therefore also a relation between the radius and mass of the pulsar. This work shows the importance of understanding the exact density limits of the pasta phase and its consequences on the choice of appropriate equations of state. More recently, a new radius-mass relation for the Vela pulsar was obtained taking as constraints recent isospin diffusion data from heavy-ion reactions [5]. In that work, both the thermodynamic and the more accurate and reliable dynamical method were utilized in order to constrain the densities and related pressures of the pasta phase present in the crust of neutron stars. The pressures were obtained from the equation of state for neutron-rich nuclear matter constrained by isospin diffusion data obtained in the same subsaturation density range as the existing ones in the neutron star crust [15].

It is, however, not clear how good the predictions are for the transition density obtained from spinodal calculations. Clusterization of the crust may have been formed through equilibrium processes, and it is important to compare spinodal results with equilibrium results, obtained from the minimization of the free energy. In Ref. [4], a first comparison revealed that as a rule the transition densities obtained within an equilibrium calculation are larger than the ones determined from the dynamical spinodals.

In the present work, we use the same approximations (CP and TF) used in Ref. [4] to obtain the pasta structures but improve on the choice of the relativistic mean-field (RMF) models; i.e., we obtain results with various density dependent hadronic models and investigate the influence of the  $\delta$  mesons. We next justify our choices.

Density dependent hadronic models [16,17] have shown to provide richer and different results in many cases than those obtained with the simpler NLWM parametrizations [18–20]. In many situations, the results are similar to the ones obtained with nonrelativistic Skyrme-type models [20–23].

The inclusion of the isovector-scalar virtual  $\delta(a_0(980))$  meson in hadronic effective field theories [24,25] influences the calculation of the effective masses with important consequences on the symmetry energy, spinodals [18], and other quantities possibly related to the appearance of the pasta phase. The  $\delta$  field introduces in the isovector channel the structure already existing in the isoscalar channel, i.e., a balance between a scalar (attractive) and a vector (repulsive) potential.

In the following study, we consider three density dependent coupling parametrizations, TW [16], DDH $\delta$  [17], and GDFM [12], and two models with constant couplings, NL3 and NL3 $\delta$ . Neither NL3 nor TW include the  $\delta$  meson. A comparison is done between the transition pressures and densities from the pasta phase to homogeneous matter obtained within the above-mentioned models and with the predictions obtained in Ref. [5].

In Sec. II, we briefly review the formalism underlying the homogeneous neutral  $npe$  matter. The pasta phase is built in Sec. III with the help of the coexisting phases method and in Sec. IV with the Thomas-Fermi approximation. In Sec. V, our results are displayed and discussed; and in Sec. VI, our conclusions are drawn.

## II. THE FORMALISM

We consider a system of protons and neutrons with mass  $M$  interacting with and through an isoscalar-scalar field  $\phi$  with mass  $m_s$ , an isoscalar-vector field  $V^\mu$  with mass  $m_v$ , an isovector-vector field  $\mathbf{b}^\mu$  with mass  $m_\rho$  and an isovector-scalar field  $\delta$  with mass  $m_\delta$ . We also include a system of electrons with mass  $m_e$ . Protons and electrons interact through the electromagnetic field  $A^\mu$ . The Lagrangian density reads

$$\mathcal{L} = \sum_{i=p,n} \mathcal{L}_i + \mathcal{L}_e + \mathcal{L}_\sigma + \mathcal{L}_\omega + \mathcal{L}_\rho + \mathcal{L}_\delta + \mathcal{L}_\gamma, \quad (1)$$

where the nucleon Lagrangian reads

$$\mathcal{L}_i = \bar{\psi}_i [\gamma_\mu i D^\mu - M^*] \psi_i, \quad (2)$$

with

$$i D^\mu = i \partial^\mu - \Gamma_v V^\mu - \frac{\Gamma_\rho}{2} \boldsymbol{\tau} \cdot \mathbf{b}^\mu - e \frac{1 + \tau_3}{2} A^\mu, \quad (3)$$

$$M^* = M - \Gamma_s \phi - \Gamma_\delta \boldsymbol{\tau} \cdot \boldsymbol{\delta}, \quad (4)$$

and the electron Lagrangian is given by

$$\mathcal{L}_e = \bar{\psi}_e [\gamma_\mu (i \partial^\mu + e A^\mu) - m_e] \psi_e. \quad (5)$$

The meson and electromagnetic Lagrangian densities are

$$\begin{aligned} \mathcal{L}_\sigma &= \frac{1}{2} (\partial_\mu \phi \partial^\mu \phi - m_s^2 \phi^2), \\ \mathcal{L}_\omega &= \frac{1}{2} (-\frac{1}{2} \Omega_{\mu\nu} \Omega^{\mu\nu} + m_v^2 V_\mu V^\mu), \\ \mathcal{L}_\rho &= \frac{1}{2} (-\frac{1}{2} \mathbf{B}_{\mu\nu} \cdot \mathbf{B}^{\mu\nu} + m_\rho^2 \mathbf{b}_\mu \cdot \mathbf{b}^\mu), \\ \mathcal{L}_\delta &= \frac{1}{2} (\partial_\mu \boldsymbol{\delta} \partial^\mu \boldsymbol{\delta} - m_\delta^2 \boldsymbol{\delta}^2), \\ \mathcal{L}_\gamma &= -\frac{1}{4} F_{\mu\nu} F^{\mu\nu}, \end{aligned}$$

where  $\Omega_{\mu\nu} = \partial_\mu V_\nu - \partial_\nu V_\mu$ ,  $\mathbf{B}_{\mu\nu} = \partial_\mu \mathbf{b}_\nu - \partial_\nu \mathbf{b}_\mu - \Gamma_\rho (\mathbf{b}_\mu \times \mathbf{b}_\nu)$ , and  $F_{\mu\nu} = \partial_\mu A_\nu - \partial_\nu A_\mu$ . The parameters of the models are the nucleon mass  $M = 939$  MeV, four density dependent coupling parameters  $\Gamma_s, \Gamma_v, \Gamma_\rho$ , and  $\Gamma_\delta$  of the mesons to the nucleons, the electron mass  $m_e$ , and the electromagnetic coupling constant  $e = \sqrt{4\pi/137}$ . In the above Lagrangian density,  $\boldsymbol{\tau}$  is the isospin operator. From the Euler-Lagrange formalism, we obtain coupled differential equations for the scalar, vector, isovector-scalar, isovector-vector, electromagnetic, and nucleon fields. In the static case, there are no currents, and the spatial vector components are zero. In Ref. [4], a complete description of the Thomas-Fermi approximation applied to different parametrizations of the NLWM is given. As the differences arising from the inclusion of the  $\delta$  mesons and the use of density dependent couplings are small, we do not repeat the equations here. A rearrangement term is the landmark of most density dependent hadronic models [26,27], and the simple mean field approximation (MFA) is outlined next so that its appearance is better understood. The equations of motion for the fields can be obtained and solved self-consistently in the MFA (the photon and meson fields are classical fields), neglecting states of negative energy (no-sea approximation) [16].

The meson fields within the mean field approximation are obtained from the equations

$$m_s^2 \phi_0 = \Gamma_s \rho_s, \quad (6)$$

$$m_v^2 V_0 = \Gamma_v \rho, \quad (7)$$

$$m_\rho^2 b_0 = \frac{\Gamma_\rho}{2} \rho_3, \quad (8)$$

$$m_\delta^2 \delta_3 = \Gamma_\delta \rho_{s3}. \quad (9)$$

The second members of these equations include the equilibrium densities  $\rho = \rho_p + \rho_n$ ,  $\rho_3 = \rho_p - \rho_n$ ,  $\rho_s = \rho_{sp} + \rho_{sn}$ , and  $\rho_{s3} = \rho_{sp} - \rho_{sn}$ , where the proton/neutron densities are given by

$$\rho_i = \frac{1}{\pi^2} \int p^2 dp (f_{i+} - f_{i-}), \quad i = p, n, \quad (10)$$

and the corresponding scalar density by

$$\rho_{si} = \frac{1}{\pi^2} \int p^2 dp \frac{M_i^*}{\sqrt{p^2 + M_i^{*2}}} (f_{i+} + f_{i-}), \quad (11)$$

with the distribution functions given by

$$f_{i\pm} = \frac{1}{1 + \exp[(\epsilon_i^*(\mathbf{p}) \mp v_i)/T]}, \quad (12)$$

where  $\epsilon_i^* = \sqrt{p^2 + M_i^{*2}}$ ,

$$M_i^* = M - \Gamma_s \phi_0 - \tau_{3i} \Gamma_\delta \delta_3, \quad (13)$$

and the effective chemical potentials are

$$v_i = \mu_i - \Gamma_v V_0 - \frac{\Gamma_\rho}{2} \tau_{3i} b_0 - \Sigma_0^R, \quad (14)$$

with  $\tau_{3i} = \pm 1$  the isospin projection for the protons and neutrons, respectively. The density dependent models in the mean field approximation contain a rearrangement term  $\Sigma_0^R$  [17]:

$$\Sigma_0^R = \frac{\partial \Gamma_v}{\partial \rho} \rho V_0 + \frac{\partial \Gamma_\rho}{\partial \rho} \rho_3 \frac{b_0}{2} - \frac{\partial \Gamma_s}{\partial \rho} \rho_s \phi_0 - \frac{\partial \Gamma_\delta}{\partial \rho} \rho_{s3} \delta_3.$$

Notice that for  $T = 0$  MeV, the distribution function for particles given in Eq. (12) becomes the simple step function  $f_i = \theta(P_{Fi}^2 - p^2)$ , and the distribution function for antiparticles vanishes.

In the description of the equations of state of a system, the required quantities are the baryonic density, energy density, pressure, and free energy. The energy density reads

$$\mathcal{E} = \sum_{i=n,p} K_i + \mathcal{E}_\sigma + \mathcal{E}_\omega + \mathcal{E}_\delta + \mathcal{E}_\rho, \quad (15)$$

with

$$K_i = \frac{1}{\pi^2} \int p^2 dp \sqrt{p^2 + M_i^{*2}} (f_{i+} + f_{i-}), \quad (16)$$

$$\mathcal{E}_\sigma = \frac{m_s^2}{2} \phi_0^2, \quad (17)$$

$$\mathcal{E}_\omega = \frac{m_v^2}{2} V_0^2, \quad (18)$$

$$\mathcal{E}_\delta = \frac{m_\delta^2}{2} \delta_3^2, \quad (19)$$

$$\mathcal{E}_\rho = \frac{m_\rho^2}{2} b_0^2. \quad (20)$$

The pressure is given by

$$P = \sum_{i=n,p} P_i + P_\sigma + P_\omega + P_\delta + P_\rho, \quad (21)$$

with the partial pressures associated with the nucleons and the various fields

$$P_i = \frac{1}{3\pi^2} \int dp \frac{p^4}{\sqrt{p^2 + M_i^{*2}}} (f_{i+} + f_{i-}),$$

$$P_\sigma = -\frac{m_s^2}{2} \phi_0^2 \left( 1 + 2 \frac{\rho}{\Gamma_s} \frac{\partial \Gamma_s}{\partial \rho} \right),$$

$$P_\omega = \frac{m_v^2}{2} V_0^2 \left( 1 + 2 \frac{\rho}{\Gamma_v} \frac{\partial \Gamma_v}{\partial \rho} \right),$$

$$P_\rho = \frac{m_\rho^2}{2} b_0^2 \left( 1 + 2 \frac{\rho}{\Gamma_\rho} \frac{\partial \Gamma_\rho}{\partial \rho} \right),$$

$$P_\delta = -\frac{m_\delta^2}{2} \delta_3^2 \left( 1 + 2 \frac{\rho}{\Gamma_\delta} \frac{\partial \Gamma_\delta}{\partial \rho} \right).$$

The free energy density is defined as

$$\mathcal{F} = \mathcal{E} - T\mathcal{S}, \quad (22)$$

with the entropy density

$$\mathcal{S} = \frac{1}{T} (\mathcal{E} + P - \mu_p \rho_p - \mu_n \rho_n). \quad (23)$$

As for the electrons, their density and distribution functions read

$$\rho_e = \frac{1}{\pi^2} \int p^2 dp (f_{e+} - f_{e-}), \quad (24)$$

with

$$f_{e\pm}(\mathbf{r}, \mathbf{p}, t) = \frac{1}{1 + \exp[(\epsilon_e \mp \mu_e)/T]}, \quad (25)$$

where  $\mu_e$  is the electron chemical potential and  $\epsilon_e = \sqrt{p^2 + m_e^2}$ . We always consider neutral matter, and therefore the electron density is equal to the proton density. In the calculation of the nonhomogeneous phase, the Coulomb energy of the proton and electron distributions is included. We study both matters (homogeneous and pasta structured), with a fixed proton fraction, as we get in heavy-ion collisions (although in this case, matter is not neutral), and in  $\beta$  equilibrium as in stellar matter. In the latter, charge neutrality conditions fix the electron chemical potential and density. The onset of muons occurs above the transition density to homogeneous phase, and therefore the proton density remains equal to the electron density.

The energy density, pressure, free energy density, and entropy density of the electrons are

$$\mathcal{E}_e = \frac{1}{\pi^2} \int dp p^2 \sqrt{p^2 + m_e^2} (f_{e+} + f_{e-}), \quad (26)$$

$$P_e = \frac{1}{3\pi^2} \int dp \frac{p^4}{\sqrt{p^2 + m_e^2}} (f_{e+} + f_{e-}), \quad (27)$$

$$\mathcal{F}_e = \mathcal{E}_e - T\mathcal{S}_e, \quad (28)$$

and

$$\mathcal{S}_e = \frac{1}{T} (\mathcal{E}_e + P_e - \mu_e \rho_e). \quad (29)$$

To obtain the equations for the TW parametrization [16] of the density dependent hadronic model, all information on the  $\delta$  meson is excluded. For the NL3 [9] parametrization, the density dependent parameters are substituted by the usual coupling constants  $g_s$ ,  $g_v$ , and  $g_\rho$ , and nonlinear parameters are included (see Ref. [4], for instance). The NL3 $\delta$  parametrization is defined with the same values for  $g_s$  and  $g_v$  as in the NL3 parametrization,  $g_\rho = 14.29$  and  $g_\delta = 7.85$ , in such a way that the symmetry energy has the same value at the saturation density as the NL3 parametrization. We show in Table I the nuclear matter properties reproduced by the models we discuss in the present work.

The density dependent coupling parameters are adjusted in order to reproduce some of the nuclear matter bulk properties, using the following parametrization for the  $\sigma$  and  $\omega$  mesons:

$$\Gamma_i(\rho) = \Gamma_i(\rho_0) h_i(x), \quad x = \rho/\rho_0, \quad (30)$$

with

$$h_i(x) = a_i \frac{1 + b_i(x + d_i)^2}{1 + c_i(x + d_i)^2}, \quad i = s, v, \quad (31)$$

TABLE I. Nuclear matter properties at the saturation density.

	NL3/NL3 $\delta$ [9]	TW [16]	DDH $\delta$ [17]	GDFM [12]
$B/A$ (MeV)	16.3	16.3	16.3	16.25
$\rho_0$ (fm $^{-3}$ )	0.148	0.153	0.153	0.178
$K$ (MeV)	272	240	240	337
$\mathcal{E}_{\text{sym}}$ (MeV)	37.4	32.0	25.1	32.11
$M^*/M$	0.60	0.56	0.56	0.68
$L$ (MeV)	117/148	55	44	57
$T_c$ (MeV)	14.55	15.18	15.18	15.95

and

$$h_\rho(x) = \exp[-a_\rho(x - 1)], \quad (32)$$

for the TW model [16]. For the DDH $\delta$  model [17], we use the TW parametrization for  $\Gamma_s$  and  $\Gamma_v$ , and for the  $\rho$  and  $\delta$  mesons we take

$$h_i(x) = a_i \exp[-b_i(x - 1)] - c_i(x - d_i), \quad i = \rho, \delta.$$

The parameters  $a_i$ ,  $b_i$ ,  $c_i$  and  $d_i$  are given in Table II, and  $\rho_0$  is the saturation density.

The density dependent parametrization (GDFM) obtained in Ref. [12] takes into account the renormalization of the relativistic mean-field theory due to Fock exchange terms. It ensures a good description of the properties of the equation of state at high density as obtained with calculations for asymmetric nuclear matter [13] with Dirac-Brueckner-Hartree-Fock calculations.

The GDFM parametrization for all four mesons coupling parameters reads

$$\Gamma_i(\rho) = a_i + (b_i + d_i x^3) \exp(-c_i x). \quad (33)$$

Around the saturation density, a correction to the coupling parameter for the  $\omega$  meson is introduced:

$$\Gamma_{\text{vcor}}(\rho) = \Gamma_v(\rho) - a_{\text{cor}} \exp\left[-\left(\frac{\rho - \rho_0}{b_{\text{cor}}}\right)^2\right], \quad (34)$$

where  $a_{\text{cor}} = 0.014$  and  $b_{\text{cor}} = 0.035$  fm $^{-3}$ . The parameters for the GDFM model are given in Table III.

The properties we discuss in the following depend on the isovector channel of the nuclear force, mainly the results obtained for  $\beta$ -equilibrium matter. Therefore we show in Fig. 1 the symmetry energy and slope of the symmetry energy  $L = 3\rho_0 \partial \epsilon_{\text{sym}} / \partial \rho$ . This quantity defined at the saturation density is given in Table I. The symmetry energy of NLW models becomes quite hard for densities above  $\sim 0.1$  fm $^{-3}$ .

TABLE III. Parameters of the GDFM model [12].

$i$	$m_i$ (MeV)	$a_i$	$b_i$	$c_i$	$d_i$
$\sigma$	550	7.7868	2.58637	2.32431	3.11504
$\omega$	782.6	9.73684	2.26377	7.05897	–
$\rho$	769	4.56919	5.45085	1.20926	–
$\delta$	983	2.68849	6.7193	0.503759	0.403927

However, at subsaturation densities, the  $\delta$  meson gives rise to softer symmetry energies; this is true for NL3 $\delta$  and for DDH $\delta$  and GDFM, with DDH $\delta$  being softer than GDFM. Looking at the slope of the symmetry energy, we see that GDFM and DDH $\delta$  show a very similar behavior. Except for TW, all models show at low densities a decrease of the slope followed by an increase of the slope above  $\rho \sim 0.05$  fm $^{-3}$  for NLW models or  $\rho \sim 0.12$  fm $^{-3}$  for density dependent models with the  $\delta$  meson. For TW, the slope always decreases with density more slowly than that for all the other models.

### III. COEXISTING PHASES

#### A. Nuclear pasta

As in Refs. [3,4], for a given total density  $\rho$  and proton fraction  $Y_p = \rho_p / \rho$ , the pasta structures are built with different geometrical forms in a background nucleon gas. This is achieved by calculating from the Gibbs conditions the density and the proton fraction of the pasta and of the background gas, so that in the whole we have to solve simultaneously the following equations:

$$P^I(v_p^I, v_n^I, M_n^{*I}, M_p^{*I}) = P^{II}(v_p^{II}, v_n^{II}, M_n^{*II}, M_p^{*II}), \quad (35)$$

$$\mu_i^I = \mu_i^{II}, \quad i = p, n, \quad (36)$$

$$m_s^2 \phi_0^I = \Gamma_s \rho_s^I, \quad (37)$$

$$m_s^2 \phi_0^{II} = \Gamma_s \rho_s^{II}, \quad (38)$$

$$m_\delta^2 \delta_3^I = \Gamma_\delta \rho_{s3}^I, \quad (39)$$

$$m_\delta^2 \delta_3^{II} = \Gamma_\delta \rho_{s3}^{II}, \quad (40)$$

$$f \rho_p^I + (1 - f) \rho_p^{II} = \rho_p = Y_p \rho, \quad (41)$$

where I and II label each of the phases,  $f$  is the volume fraction of phase I,

$$f = \frac{\rho - \rho^{II}}{\rho^I - \rho^{II}}, \quad (42)$$

and  $Y_p$  is the global proton fraction. The density of electrons is uniform and taken as  $\rho_e = Y_p \rho$ . For the NL3 and NL3 $\delta$

TABLE II. Parameters of the TW [16] and DDH $\delta$  models [17,18].

$i$	$m_i$ (MeV)	$\Gamma_i(\rho_0)$	$a_i$	$b_i$	$c_i$	$d_i$
$\sigma$	550	10.72854	1.365469	0.226061	0.409704	0.901995
$\omega$	783	13.29015	1.402488	0.172577	0.344293	0.983955
$\rho_{\text{TW}}$	763	7.32196	0.515	–	–	–
$\rho_{\text{DDH}\delta}$	763	11.727	0.095268	2.171	0.05336	17.8431
$\delta$	980	7.58963	0.01984	3.4732	–0.0908	–9.811

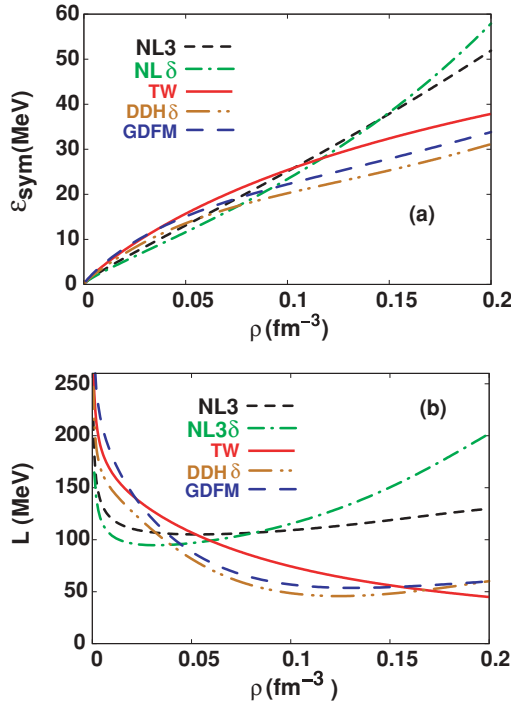


FIG. 1. (Color online) (a) Symmetry energy and (b) slope of symmetry energy for the models under study.

parametrizations, nonlinear  $\sigma$  terms must be included in Eqs. (37) and (38).

The total pressure is given by  $P = P^I + P_e$ . The total energy density of the system is given by

$$\mathcal{E} = f\mathcal{E}^I + (1-f)\mathcal{E}^{II} + \mathcal{E}_e + \mathcal{E}_{\text{surf}} + \mathcal{E}_{\text{Coul}}, \quad (43)$$

where, by minimizing the sum  $\mathcal{E}_{\text{surf}} + \mathcal{E}_{\text{Coul}}$  with respect to the size of the droplet/bubble, rod/tube or slab, we get [3]  $\mathcal{E}_{\text{surf}} = 2\mathcal{E}_{\text{Coul}}$ , and

$$\mathcal{E}_{\text{Coul}} = \frac{2\alpha}{4^{2/3}} (e^2 \pi \Phi)^{1/3} [\sigma D (\rho_p^I - \rho_p^{II})]^2, \quad (44)$$

where  $\alpha = f$  for droplets and  $\alpha = 1 - f$  for bubbles,  $\sigma$  is the surface energy coefficient, and  $D$  is the dimension of the system. For droplets, rods, and slabs,

$$\Phi = \begin{cases} \left( \frac{2-Df^{1-2/D}}{D-2} + f \right) \frac{1}{D+2}, & D = 1, 3, \\ \frac{f-1-\ln(f)}{D+2}, & D = 2, \end{cases} \quad (45)$$

and for bubbles and tubes the above expressions are valid with  $f$  replaced by  $1 - f$ .

Concerning the surface energy, the authors of Ref. [3] state that, in this case, the appearance of the pasta phase essentially depends on the value of the surface tension. We fixed the surface tension at different values and confirmed their claim. We parametrized the surface energy coefficient in terms of the proton fraction according to the functional proposed in Ref. [28], which was obtained by fitting Thomas-Fermi and Hartree-Fock numerical values with a Skyrme force,

$$\sigma = \sigma_0 \frac{16 + b}{\frac{1}{Y_p^3} + \frac{1}{(1-Y_p)^3} + b} h_t, \quad (46)$$

with

$$h_t = \left[ 1 - \left( \frac{T}{4T_c Y_p (1 - Y_p)} \right)^2 \right]^2, \quad (47)$$

$\sigma_0 = 1.03 \text{ MeV}/\text{fm}^2$ ,  $b = 24.4$ , and  $T_c$  is the critical temperature above which there is a smooth transition from the gas phase to the liquid phase [19] (given in Table I). We have checked that small variations of this temperature do not affect our results. The proton fraction considered throughout the calculation of  $\sigma$  is the one of the denser phases.

Each structure is considered to be in the center of a charge neutral Wigner-Seitz cell composed of neutrons, protons, and leptons [29]. The Wigner-Seitz cell is a sphere/cylinder/slab whose volume is the same as the unit body centered cubic (BCC) cell. In Ref. [29], the internal structures are associated with heavy nuclei. Hence, the radii of the droplet (rod, slab) and the Wigner-Seitz cell are, respectively, given by

$$R_D = \left( \frac{\sigma D}{4\pi e^2 (\rho_p^I - \rho_p^{II})^2 \Phi} \right)^{1/3}, \quad R_W = \frac{R_D}{(1-f)^{1/D}}. \quad (48)$$

## B. Stellar pasta

In this case, hadronic matter is in  $\beta$  equilibrium. The condition of  $\beta$  equilibrium in a system of protons, neutrons, electrons, and muons is

$$\mu_p = \mu_n - \mu_e, \quad (49)$$

where  $\mu_e = \mu_\mu$ . As the muons are added, the imposition of charge neutrality requires that

$$\rho_p = \rho_e + \rho_\mu. \quad (50)$$

The Gibbs conditions to be enforced are

$$\mu_n^I = \mu_n^{II}, \quad \mu_e^I = \mu_e^{II}, \quad (51)$$

and

$$f(\rho_p^I - \rho_e^I - \rho_\mu^I) + (1-f)(\rho_p^{II} - \rho_e^{II} - \rho_\mu^{II}) = 0, \quad (52)$$

together with Eqs. (35), (37)–(40). Here, the density of electrons is no longer taken to be uniform as in the last section, but appears as the solution of Eq. (52). The densities of interest to the study of the pasta phase are too low for the muons to appear, which generally occurs for densities above  $0.1 \text{ fm}^{-3}$  [23].

## IV. PASTA PHASE WITHIN THE THOMAS-FERMI APPROXIMATION

In the present work, we repeat the same numerical prescription given in Ref. [4]; that is, within the Thomas-Fermi approximation of the nonuniform  $npe$  matter, the fields are assumed to vary slowly so that the baryons can be treated as moving in locally constant fields at each point. In the Thomas-Fermi approximation, the energy is a functional of

the density given by

$$E_{\text{TF}} = \int d^3r \left( \sum_{i=p,n,e} E_i(\mathbf{r}) + \frac{1}{2} [(\nabla\phi_0(\mathbf{r}))^2 + m_s^2\phi_0^2(\mathbf{r})] - \frac{1}{2} [(\nabla V_0(\mathbf{r}))^2 + m_v^2 V_0^2(\mathbf{r})] - \frac{1}{2} [(\nabla b_0(\mathbf{r}))^2 + m_\rho^2 b_0^2(\mathbf{r})] + \frac{1}{2} [(\nabla\delta_3(\mathbf{r}))^2 + m_\delta^2\delta_3^2(\mathbf{r})] + \Gamma_v V_0(\mathbf{r})\rho + \frac{1}{2}\Gamma_\rho b_0(\mathbf{r})\rho_3 - \frac{1}{2} [\nabla A_0(\mathbf{r})]^2 + e(\rho_p - \rho_e)A_0(\mathbf{r}) \right), \quad (53)$$

where

$$E_i = \frac{1}{\pi^2} \int_0^{p_{F_i}(\mathbf{r})} dp p^2 (p^2 + M_i^{*2})^{1/2}, \quad i = p, n, \quad (54)$$

and

$$E_e = \frac{1}{\pi^2} \int_0^{p_{F_e}(\mathbf{r})} dp p^2 (p^2 + m_e^2)^{1/2}. \quad (55)$$

The definition of the thermodynamic potential reduces to

$$\Omega = E_{\text{TF}}[\rho_i] - \sum_{i=n,p,e} \mu_i \int dr \rho_i(\mathbf{r}). \quad (56)$$

The minimization of the above functional with the constraint of a fixed number of protons, neutrons, and electrons yields the equations

$$(p_{F_p}^2(\mathbf{r}) + M_p^{*2}(\mathbf{r}))^{1/2} + \Gamma_v V_0(\mathbf{r}) + \frac{1}{2}\Gamma_\rho b_0(\mathbf{r}) + \Sigma_0^R + eA_0(\mathbf{r}) = \mu_p, \quad (57)$$

$$(p_{F_n}^2(\mathbf{r}) + M_n^{*2}(\mathbf{r}))^{1/2} + \Gamma_v V_0(\mathbf{r}) - \frac{1}{2}\Gamma_\rho b_0(\mathbf{r}) + \Sigma_0^R = \mu_n, \quad (58)$$

where  $M_p^*$  and  $M_n^*$  are given in Eq. (13) and

$$(p_{F_e}^2(\mathbf{r}) + m_e^2)^{1/2} - eA_0(\mathbf{r}) = \mu_e. \quad (59)$$

The numerical algorithm for the description of the neutral  $npe$  matter was discussed in detail in Ref. [4]. The Poisson equation is always solved by using the appropriate Green's function according to the spatial dimension of interest, and the Klein-Gordon equations are solved by expanding the meson fields in a harmonic oscillator basis with one, two, or three dimensions based on the method proposed in Ref. [30].

## V. RESULTS AND DISCUSSIONS

We show and discuss the results obtained using the coexistence-phases (CP) and Thomas-Fermi (TF) methods in the framework of the several relativistic models presented, always for  $npe$  matter. We start with the results at  $T = 0$  MeV.

In Fig. 2, results for a homogeneous description of matter are compared with the output of the CP calculation for two proton fractions. We see that all the models predict the existence of a nonhomogeneous pasta phase: in models with constant couplings, NL3 and NL3 $\delta$ , this phase clearly decreases if  $y_p$  decreases (higher asymmetries); a different behavior occurs for density dependent coupling models where the nonhomogeneous phase extends to higher densities and may even increase when the proton fraction reduces. From Table IV, one can see that the TF method also predicts for density dependent coupling models either a small increase (DDH $\delta$ ) or just a small decrease (TW) of the extension of the pasta phase, if we decrease the proton fraction from 0.5 to 0.3. The GDFM model presents a large pasta phase at both

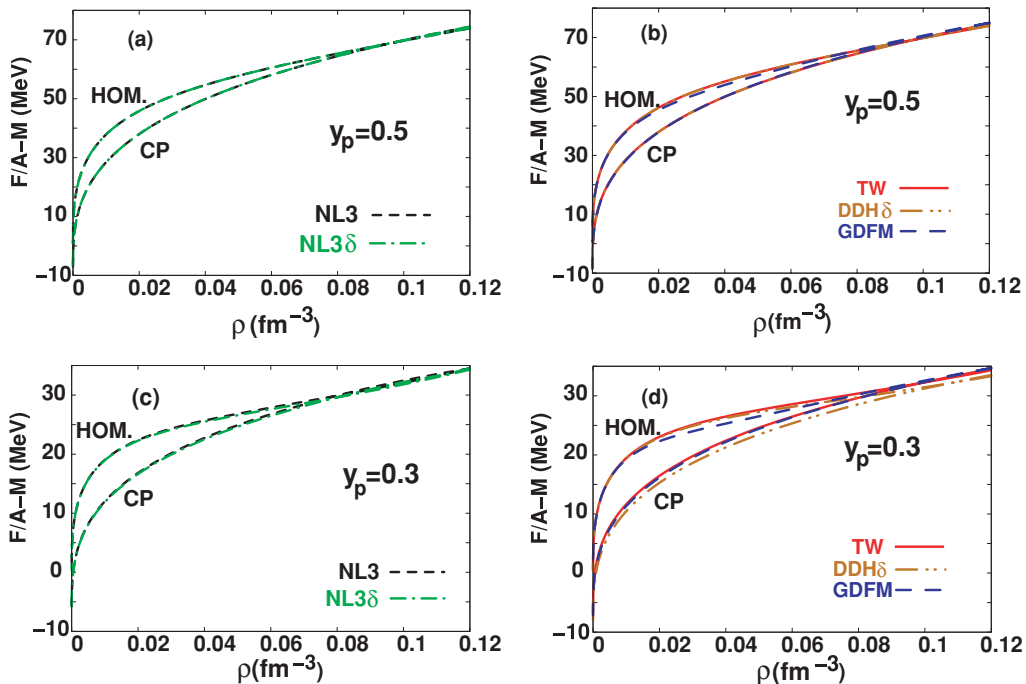


FIG. 2. (Color online)  $npe$  matter (pasta + homogeneous phase) energy per particle at  $T = 0$  MeV for RMF models with constant couplings [(a), (c)] and density dependent coupling models [(b), (d)]:  $y_p = 0.5$  (top),  $y_p = 0.3$  (bottom).

TABLE IV. Transition densities in  $\text{fm}^{-3}$  and corresponding pressures (CP and TF calculations) for the nonhomogeneous to homogeneous phase at the inner edge of the crust ( $T = 0$ ) MeV.

Model	EOS	Dynamic spinodal vs EOS	Thermodynamic spinodal vs EOS	Pasta (CP) vs uniform matter	$P$ (CP) ( $\text{MeV}/\text{fm}^3$ )	Pasta (TF) vs uniform matter	$P$ (TF) ( $\text{MeV}/\text{fm}^3$ )
NL3	$y_p = 0.5$	0.083	0.096	0.096	2.65	0.112	2.64
NL3	$y_p = 0.3$	0.080	0.094	0.079	1.05	0.100	1.14
NL3	$\beta$ equil.	0.053	0.065	–	–	0.054	0.24
NL3 $\delta$	$y_p = 0.5$	0.083	0.096	0.096	2.65	0.112	2.64
NL3 $\delta$	$y_p = 0.3$	0.079	0.093	0.080	1.06	0.099	1.14
NL3 $\delta$	$\beta$ equil.	0.048	0.056	–	–	0.051	0.16
TW	$y_p = 0.5$	0.083	0.096	0.098	2.74	0.113	2.66
TW	$y_p = 0.3$	0.084	0.095	0.099	1.40	0.111	1.27
TW	$\beta$ equil.	0.075	0.085	0.060	0.26	0.076	0.40
DDH $\delta$	$y_p = 0.5$	0.083	0.096	0.098	2.74	0.113	2.66
DDH $\delta$	$y_p = 0.3$	0.084	0.094	0.107	1.55	0.115	1.29
DDH $\delta$	$\beta$ equil.	0.079	0.085	0.089	0.17	0.079	0.10
GDFM	$y_p = 0.5$	0.133	0.141	0.119	3.55	0.144	3.81
GDFM	$y_p = 0.3$	0.131	0.138	0.119	1.79	0.140	1.83
GDFM	$\beta$ equil.	0.051	0.058	0.027	0.04	0.052	0.13

asymmetries, but it is with the DDH $\delta$  model that the most variety of pasta structures can be observed (see Fig. 3).

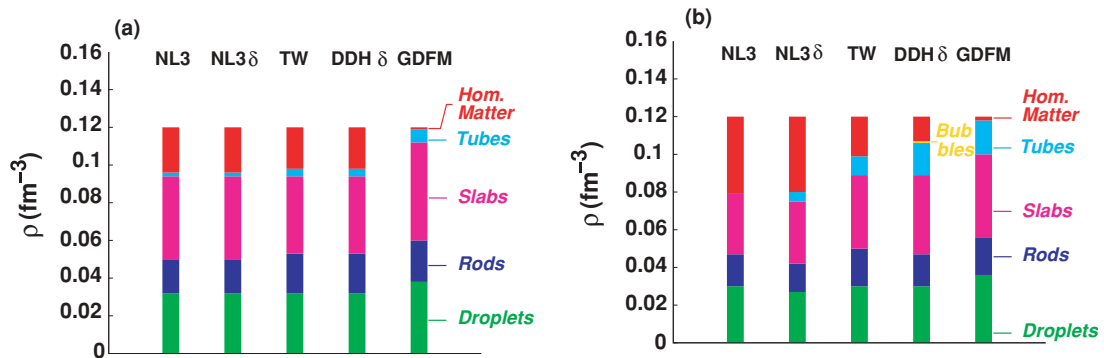
We also point out that models NL3 and NL3 $\delta$  as well as TW and DDH $\delta$  show the same transition densities for  $y_p = 0.5$ , because the effect of the  $\delta$  meson is only seen for asymmetric matter for the CP and spinodal calculations. Both model pairs have the same coupling constants for the  $\sigma$  and the  $\omega$  mesons and only differ in the isovector channel, namely, the  $\rho$  and  $\delta$  meson couplings. However, in the TF calculation, the distribution of protons and neutrons is free to adjust itself to the lowest energy configuration. As a consequence, the proton and neutron density distributions do not coincide within the Wigner-Seitz cell, and the  $\rho$  and  $\delta$  fields are not zero. However, the differences are not large enough to change the transition density, and we still get the same transition density within TF, for  $y_p = 0.5$  and the model pairs (NL3, NL3 $\delta$ ) and (TW, DDH $\delta$ ).

For matter in  $\beta$  equilibrium at  $T = 0$  MeV, the energy per particle for the pasta is always slightly larger than for

the corresponding homogeneous matter in the models with constant couplings within the CP method; so, in these cases, the pasta is never preferred to represent the ground state of the system. The absence of a pasta phase in the NL3 and NL3 $\delta$  parametrizations is related to the very high values of the surface tension coefficient  $\sigma$  for these models, as can be seen in Fig. 4.

For the DDH models, we show in Fig. 5 that these models predict nonhomogeneous phases occurring for a relatively small range of densities (below  $\rho \sim 0.027 \text{ fm}^{-3}$ ) for the GDFM model but extending up to  $\rho \sim 0.09 \text{ fm}^{-3}$  in DDH $\delta$ . TW shows an intermediate behavior. Because of the low symmetry energy of the DDH $\delta$  model, which is only 25 MeV at saturation density, it was shown in Ref. [31] that  $\beta$ -equilibrium matter would even present at low densities a range of densities with a negative compressibility. This behavior favors the appearance of a larger variety of cluster forms.

Surface tension depends on the proton fraction of the high-density region inside the Wigner-Seitz cell. Models with


 FIG. 3. (Color online) Comparison of the phase diagrams at  $T = 0$  MeV for (a)  $y_p = 0.5$  and (b)  $y_p = 0.3$  obtained with the CP method for several models.

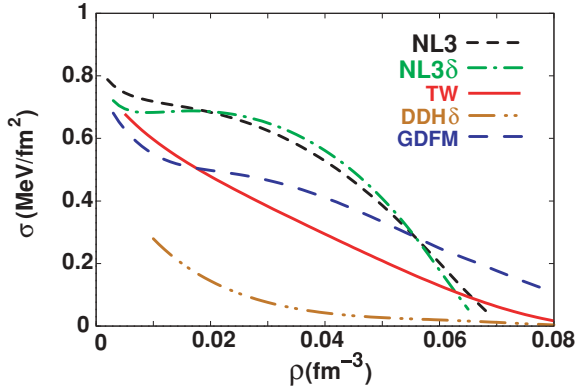


FIG. 4. (Color online) Surface tension coefficient  $\sigma$  at  $T = 0$  MeV calculated according to Eq. (46).

a larger symmetry energy give a dense region with a larger proton fraction and therefore a larger surface energy [see Eq. (46)]. We also confirm that DDH $\delta$  shows the smallest values for this quantity. Within the TF method, on the other hand, the pasta phase is also found with the models bearing constant couplings. This is because in the TF approach the surface energy is calculated self-consistently and is not introduced by hand. We know, however, that the TF approach predicts a too steep surface; therefore, we may expect that a quantal approach would predict a larger pasta phase [20].

The spinodal surface gives information about the minimal dimension of the pasta phase. A spinodal decomposition would be expected in the case of a fast transition; however, in stellar matter we may expect that there is always plenty of time to achieve equilibration. In Ref. [5], it was shown that the thermodynamic spinodal results for  $pn$  matter did not differ very much from the dynamic spinodal ones for  $npe$  matter. This seems to indicate that the Coulomb interaction and surface tension do not influence the pasta phase extension very much. The thermodynamic spinodal for  $npe$  matter either does not exist for density dependent hadronic models or is very small for NLW models because of the large incompressibility of electrons. However, although thermodynamically stable,  $npe$

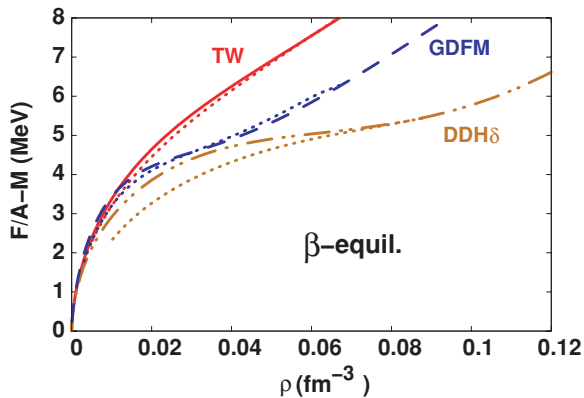


FIG. 5. (Color online)  $npe$  matter energy per particle at  $T = 0$  MeV for DDH models at  $\beta$  equilibrium. The full, dashed, and dot-dot dashed lines stand for homogeneous matter; and the corresponding dotted lines, for pasta phases.

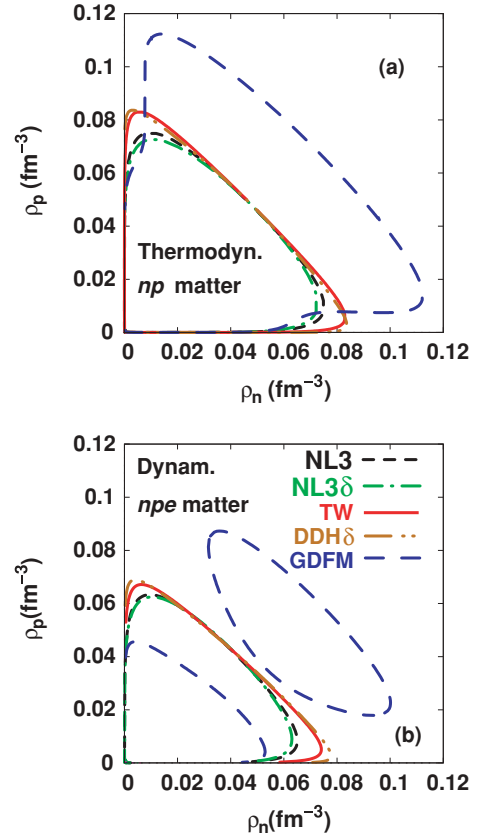


FIG. 6. (Color online) (a) Thermodynamic spinodal for  $np$  matter and (b) dynamic spinodal for  $npe$  matter, for a transfer momentum  $k = 80$  MeV, for all the models under study.

matter clusterizes as soon as it suffers a density fluctuation due to any kind of perturbation. Therefore we discuss the extension of the nonhomogeneous phase by analyzing the dynamical spinodal for  $npe$  matter, within the several models considered.

In Fig. 6, we display both the thermodynamic spinodals for  $np$  matter and the dynamical spinodals for  $npe$  matter for a momentum transfer  $k = 80$  MeV, which essentially defines the envelope of the spinodal surfaces for all  $k$  values [32]. The dynamical spinodals are smaller than the thermodynamic ones, as expected. The crossing densities of the EOS with a fixed proton fraction equal to 0.5 and 0.3 and for  $\beta$ -equilibrium matter are given in Table IV.

A larger extension of the pasta phase within the GDFM model is expected from the thermodynamic spinodal, which we show in Fig. 6. We notice that GDFM has a very peculiar behavior with a much larger thermodynamic spinodal. There is, however, an intermediate density region where matter is not so unstable and the presence of electrons is enough to raise the instability giving origin to two disconnected unstable regions. Comparing all the spinodals, we expect smaller nonhomogeneous regions for NL3 $\delta$  and a larger one for GDFM if  $y_p$  is not too small. For very asymmetric matter such as matter in  $\beta$  equilibrium, the TW and DDH $\delta$  models bear the largest pasta phases, and NL3, NL3 $\delta$ , and GDFM predict similar results. We also verify that the dynamical spinodal

predicts a slight increase of the unstable region when  $y_p$  decreases from 0.5 to 0.3. This behavior is directly related to the concavity of the spinodal at  $y_p = 0.5$ . In Ref. [23], it was seen that the concavity of the thermodynamic spinodal for the TW parametrization at  $y_p = 0.5$  is smaller than the one obtained with the NLWM. The presence of electrons and the Coulomb field in the calculation of the dynamical spinodal gives rise to a spinodal that is not symmetric with respect to the  $y_p = 0.5$  axis. The spinodal may extend to larger densities for smaller proton fractions and the same isospin asymmetry. As discussed in Ref. [33], we also expect a larger extension of the nonhomogeneous phase if the electron contribution is described correctly and the Coulomb field is included self-consistently, which stabilizes  $npe$  matter and extends the nonhomogeneous phase.

It is interesting to compare the density transitions obtained within the spinodal approaches with the corresponding values determined from the minimization of the free energy within both the CP and TF approaches. As discussed before, the dynamical spinodals are expected to indicate a lower limit. Within the present models, the transition densities obtained from the thermodynamic spinodal are  $\sim 10\text{--}15\%$  larger than the values obtained from the dynamical spinodal, similar to the conclusion drawn in Ref. [5]. For the proton fractions 0.5 and 0.3, these values are always larger than the ones obtained within an equilibrium calculation, either CP or TF, except for the GDFM model for which the CP results are smaller than the spinodal ones. For the  $\beta$ -equilibrium calculation, the CP method predicts no pasta phase for the NLWM parametrizations (NL3 and NL3 $\delta$ ). This is due to the non-self-consistent description of the surface in the CP approach. The TF approach, which treats the surface self-consistently, predicts, for all models, a transition density larger than, but very similar to, the one predicted by the dynamical spinodal calculation. This result is very interesting, because it implies that to calculate the transition density at the inner edge of the compact star crust, it is enough to use a dynamical spinodal calculation.

In Table V, we compare the transition densities between the different pasta geometries obtained in the present calculation with the results from Ref. [12], where both a TF and a microscopic calculation were done. In the TF calculation, the surface description was not fully self-consistent because it involved the inclusion of a surface energy parameter that was adjusted to reproduce the experimental binding energy of the nucleus  $^{208}\text{Pb}$ . We conclude that with a self-consistent TF calculation, the transition densities between the different geometries and from nonhomogeneous to homogeneous matter

TABLE V. Transition densities in  $\text{fm}^{-3}$  between the different geometries at  $T = 0$  MeV and for the GDFM model. Comparison with the results from Ref. [12].

	CP	TF	TF [12]	H [12]
Droplet-rod		0.047	0.048	0.052
Rod-slab		0.048	–	–
Slab-hom.	0.027	0.052	0.061	0.064

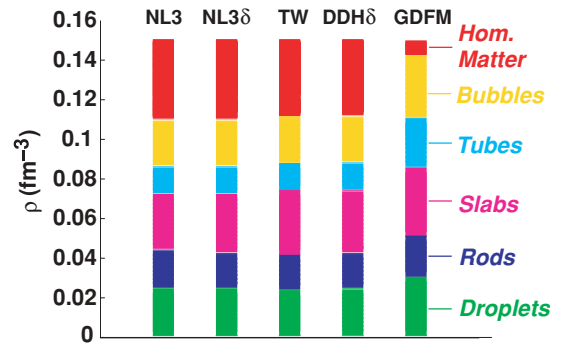


FIG. 7. (Color online) Phase diagrams at  $T = 0$  MeV and  $y_p = 0.5$  obtained with the TF method for several models.

are quite smaller than the results in Ref. [12] obtained within a microscopic description of the pasta structures including pairing effects. This comparison should also be done for different proton fractions and not only for  $\beta$ -equilibrium matter.

From the phase diagrams shown in Figs. 3(a) and 3(b), we observe that most models predict the formation of inhomogeneities of the type droplet, rod, slab, and tube for the asymmetries considered. For  $y_p = 0.3$ , only NL3 evolves to homogeneous matter without a tube-like structure, and, on the other side, DDH $\delta$  predicts the appearance of bubbles in a narrow interval of densities. These differences are due to the dependence of the surface energy on the proton asymmetry and on the slope of the symmetry energy. In Fig. 7, the phase diagrams obtained with the TF method for the models under study are displayed with  $y_p = 0.5$ . In this case, the bubble structure, not present in Fig. 3(a), appears. The transition densities are systematically higher with TF than with CP, as seen in Table IV, and therefore another phase structure is accommodated.

At this point, we compare our results shown in Table IV for  $npe$  matter in  $\beta$  equilibrium with the predictions given in Ref. [5]. According to Ref. [5], the transition density and pressure from the liquid core to the solid crust at the inner edge of neutron stars should lie within the ranges

$$0.04 \leq \rho \leq 0.065 \text{ fm}^{-3}, \quad 0.01 \leq P \leq 0.26 \text{ MeV/fm}^3. \quad (60)$$

The values for the pressure were constrained to the values for the slope of the symmetry energy at the saturation density given by  $L = 86 \pm 25$  MeV. The limits on the transition pressure defined in Ref. [5] are, however, quite smaller than the ones given in Ref. [14], namely,  $0.25 \leq P \leq 0.65$  MeV/fm $^3$ , obtained from realistic EOS.

One can see in Table I that the NL3 and NL3 $\delta$  models have  $L$  values, respectively, slightly larger and larger than the upper limit of the proposed  $L$  values. However, using the TF method, we get for the transition densities and related pressures from the pasta phase to the homogeneous phase, values within the proposed range. On the other hand, the density dependent models have  $L$  values slightly smaller than the lower limit of the above  $L$  range.

In Ref. [34], a systematic analysis of the pasta regime in terms of  $L$  was performed. The authors concluded that the presence (or absence) of the pasta phase is controlled by this

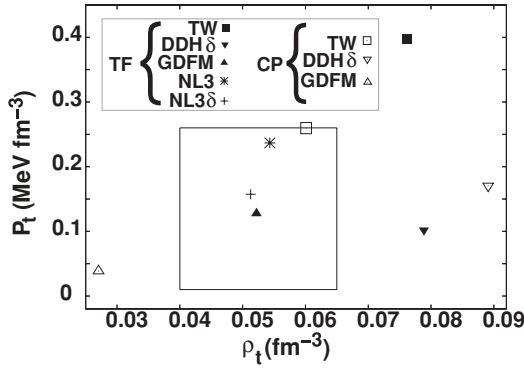


FIG. 8. Density and pressure of the inner edge that divides the liquid core from the solid crust of neutron stars according to Ref. [5].

parameter, and the pasta phase was shown to appear in neutron star matter when  $L \leq 100$  MeV. This prediction coincides only with our findings with the CP method, as can be seen from Tables I and IV.

The results for the transition pressure and density in the TW model lie just at the border of the rectangle that sets the limits given in Eqs. (60) for the CP calculation, but they become too high when the TF method is used. For the DDH $\delta$  parameter set, the results for the pressure are inside the range shown in Eqs. (60) both in the CP and TF approaches. However, for this model, the transition density is too high for both calculations. For the GDFM parametrization, the density within the CP method is not good since it comes up too low, but the TF results lie within the imposed constraints. For the NL3 and NL3 $\delta$  parametrizations, the pasta phase is only obtained within the TF results, and they come out inside the constrained range. These observations are summarized in Fig. 8.

Within the dynamical spinodal calculation, the transition densities for TW and DDH $\delta$  are high, but all the other models are within the density range given in Eqs. (60).

Also from Table IV one observes that the influence of the  $\delta$  meson is only effective for large proton asymmetries. For proton fractions 0.5 and 0.3, NL3 and NL3 $\delta$  give similar results. The effect of the  $\delta$  meson is only observed in the  $\beta$ -equilibrium matter results: for the constant coupling models the inclusion of the  $\delta$ -meson makes the pasta phase range a bit smaller, the results of the TF calculation being in good agreement with the dynamical spinodal ones. Among the density dependent models and considering all type of calculations presented, we see that the extension of the pasta phase for DDH $\delta$  is larger than the corresponding one within TW which does not include the  $\delta$  mesons. This is due to the low value of the symmetry energy within the DDH $\delta$  model.

We now comment on the results with finite temperature, all of them obtained with the CP method. In Fig. 9, we plot the free energy per particle for the models with constant couplings. As expected from the  $T = 0$  MeV results, no pasta phase appears when  $\beta$  equilibrium is enforced. For fixed proton fractions (0.5 and 0.3), the pasta phase shrinks with temperature. At very low densities, the homogeneous phase has a lower free energy than the pasta phase.

This behavior had already been noticed in Ref. [4] and is reproduced with DDH parametrizations, as seen in Fig. 10 for  $y_p = 0.5, 0.3$  and for matter in  $\beta$  equilibrium. From Figs. 10 and 11, it is seen that the size of the pasta phase depends on the asymmetry of the  $npe$  matter and on the chosen parametrization. Just two models provide pasta phase within CP for matter in  $\beta$  equilibrium at  $T = 5$  MeV: TW and DDH $\delta$ , the second being larger than the first.

In Table VI, the transition densities obtained within the CP approach and using the thermodynamic spinodal are given. No data for a dynamical spinodal calculation at finite temperature are available, except for NL3, see Ref. [4], where the transition densities  $0.080, 0.077 \text{ fm}^{-3}$  were given, respectively, for  $y_p = 0.5$  and  $0.3$  at  $T = 5$  MeV. In this case, no crossing occurs for  $\beta$ -equilibrium matter. These values are similar to the ones obtained within the CP calculation. As discussed before,

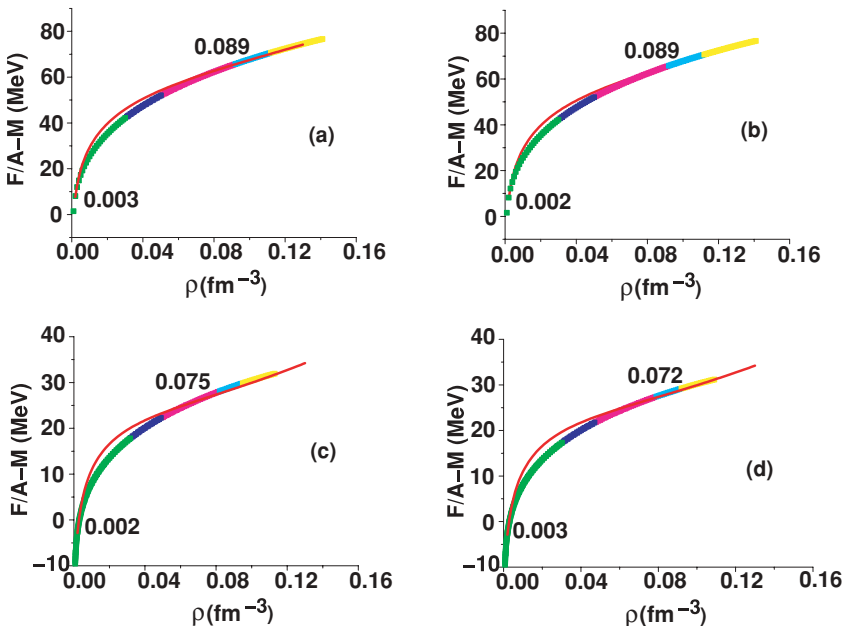


FIG. 9. (Color online)  $npe$  matter (pasta + homogeneous phases) free energy per particle at  $T = 5$  MeV for RMF models with constant couplings: NL3 [(a) and (c)] and NL3 $\delta$  [(b) and (d)].  $y_p = 0.5$  (top),  $y_p = 0.3$  (bottom).

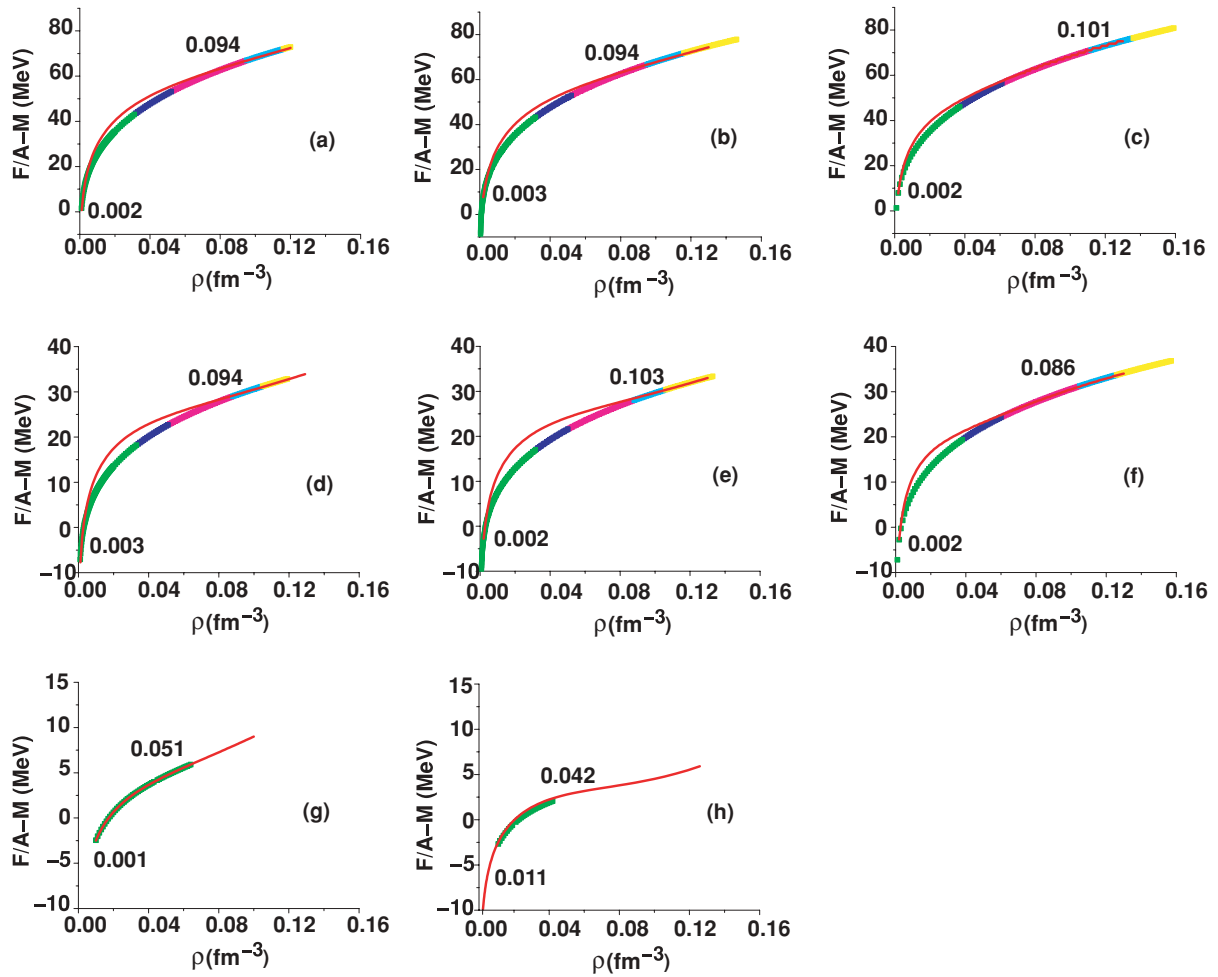


FIG. 10. (Color online) *npe* matter (pasta + homogeneous phase) free energy per particle at  $T = 5$  MeV for RMF models with density dependent couplings: TW [(a), (d), and (g)], DDH $\delta$  [(b), (e), and (h)], GDFM [(c) and (f)].  $y_p = 0.5$  (top),  $y_p = 0.3$  (middle), and  $\beta$  equilibrium (bottom).

we expect that the dynamical spinodal defines a lower limit for the transition density. From the discussion of the results obtained for the pasta phase at  $T = 0$  MeV, we also expect that the CP calculation only gives a lower limit for the transition density because of the description of the surface which takes too large values. The thermodynamic spinodal only suggests

an order of magnitude, which, according to Ref. [4] and for NL3, was always a bit larger than the values coming from the CP approach and closer to the TF results for the NLW models.

For the DDH models, it is seen that within the CP approach, and similarly to the result already discussed at  $T = 0$  MeV, the pasta phase at  $T = 5$  MeV does not decrease when going from

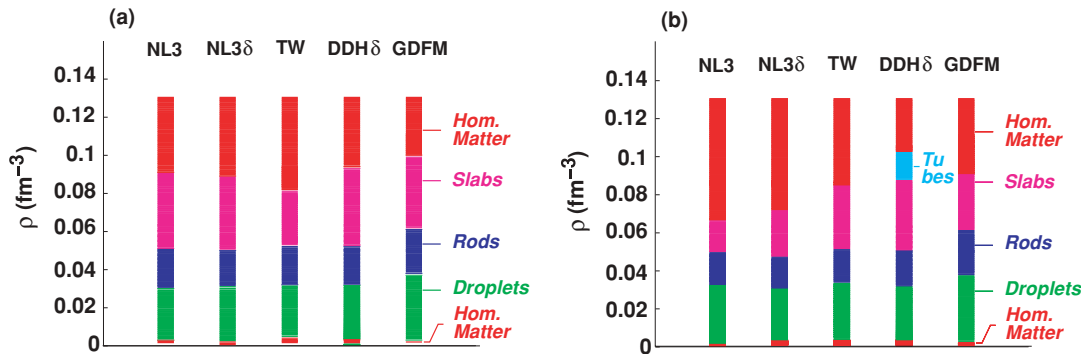


FIG. 11. (Color online) Comparison of the phase diagrams at  $T = 5$  MeV for (a)  $y_p = 0.5$  and (b)  $y_p = 0.3$  obtained with the CP method for several models.

TABLE VI. Transition densities in  $\text{fm}^{-3}$  and corresponding pressures (CP calculation) for the nonhomogeneous to homogeneous phase at the inner edge of the crust ( $T = 5$  MeV).

Model	EOS	Thermodynamic spinodal vs EOS	Pasta (CP) vs EOS	$P$ (CP) (MeV/ $\text{fm}^3$ ) uniform matter
NL3	$y_p = 0.5$	0.094	0.089	2.42
NL3	$y_p = 0.3$	0.090	0.075	1.02
NL3	$\beta$ equil.	–	–	–
NL3 $\delta$	$y_p = 0.5$	0.094	0.089	2.41
NL3 $\delta$	$y_p = 0.3$	0.090	0.072	0.96
NL3 $\delta$	$\beta$ equil.	–	–	–
TW	$y_p = 0.5$	0.095	0.094	2.59
TW	$y_p = 0.3$	0.094	0.094	0.94
TW	$\beta$ equil.	0.051	0.035	0.15
DDH $\delta$	$y_p = 0.5$	0.095	0.094	2.59
DDH $\delta$	$y_p = 0.3$	0.093	0.103	1.51
DDH $\delta$	$\beta$ equil.	0.073	0.042	0.10
GDFM	$y_p = 0.5$	0.140	0.101	2.84
GDFM	$y_p = 0.3$	0.137	0.086	1.20
GDFM	$\beta$ equil.	0.029	–	–

$y_p = 0.5$  to  $y_p = 0.3$  for both the TW and DDH $\delta$  models. It is also seen that for symmetric matter, the prediction obtained from the thermodynamic spinodal is generally quite larger than the values obtained within the CP calculation, except for the DDH $\delta$  model, when they are similar. This may indicate that within a TF calculation, larger transition densities would be obtained.

Self-consistent calculations at finite temperature, both for the pasta phase and for the dynamical spinodal, still have to be implemented. These are of particular interest because neutrino trapping occurs at finite temperature, and we expect that the interaction of neutrinos with the  $npe$  clusters may affect the neutrino energy deposition in stellar matter. However, while the CP calculation fails to predict the transition densities for  $\beta$ -equilibrium matter, we expect that it gives reasonable results for the proton fractions of interest for stellar matter with trapped neutrinos,  $y_p \sim 0.3$ .

We show in Table VII the highest temperatures for the existence of the pasta phase for each of the models discussed in this work within the CP approach. We take these values as lower bounds for the limit temperature above which the nonhomogeneous phase disappears. It is also worth mentioning that we have searched for the pasta structures at temperature steps of 1 MeV, due to the uncertainties mentioned

above, and therefore the limiting temperature given is not more than an order of magnitude. Two different situations had to be considered when the homogeneous phase was taken as the equilibrium configuration: (a) the pasta phase exists but is not the preferential state of matter, because its free energy comes out higher than the homogeneous phase, and (b) the pasta phase does not exist within the precision of our calculations.

## VI. CONCLUSIONS

In the present work, we have investigated the extension of the pasta phase for  $npe$  matter described within relativistic density dependent models, namely, TW [16], DDH $\delta$  [17], and GDFM [12], both at zero and finite temperatures. The pasta phase was calculated at zero temperature within the Thomas-Fermi method and compared with results obtained in a simplified approach, the coexistence phases (CP) method [4]. Because of the approximate way the surface is described within the CP approach, the pasta phase comes out smaller than with TF: as in Ref. [4], we conclude that a correct description of the surface energy and its dependence on the isospin, temperature, and geometry is essential to obtaining better results using the CP formalism.

The effect of including the  $\delta$  meson was also explicitly investigated: together with DDH $\delta$  and GDFM we have also considered NL3 $\delta$ . It was seen that models with the same description of the isoscalar channel and the same symmetry energy at the saturation density, namely, the pair (NL3, NL3 $\delta$ ), showed a smaller nonhomogeneous phase for asymmetric matter when the  $\delta$  meson was included. This effect does not occur for the pair (TW, DDH $\delta$ ), because although both have the same description of the isoscalar channel, the symmetry energy of the DDH $\delta$  at saturation is smaller. As a result, the

TABLE VII. Highest temperatures for which pasta phase was found in MeV.

	NL3 [9]	NL3 $\delta$	TW [16]	DDH $\delta$ [17]	GDFM [12]
$y_p = 0.5$	12.0	12.0	14.0	14.0	10.0
$y_p = 0.3$	10.0	7.0	13.0	12.0	8.0
$\beta$ equil.	–	–	5.0	8.0	4.0

extension of the nonhomogeneous phase within the DDH $\delta$  model is the largest one for  $\beta$ -equilibrium stellar matter and is larger than the corresponding nonhomogeneous phase within the TW model.

Results were compared with previous studies done within NLWM and the predictions obtained from the analysis of the thermodynamic and dynamic spinodals. One of the main conclusions is that density dependent hadronic models generally predict larger nonhomogeneous phases for asymmetric matter than NLW models. In fact, for  $\beta$ -equilibrium matter, a similar conclusion had been taken in Ref. [23] only from the analysis of the crossing of the  $\beta$ -equilibrium EOS with the dynamical spinodal. Recent parametrizations of the Skyrme force, e.g., SLy230a, NRAPR, or LNS, showed a similar behavior [23]. We confirm this behavior within both the CP and TF calculations.

One important conclusion obtained at  $T = 0$  MeV is that the transition density for  $\beta$ -equilibrium matter obtained within a TF calculation almost coincides with the prediction from the dynamical spinodal. This fact should be confirmed at finite temperature. However, for symmetric matter or for isospin asymmetries not much smaller than  $y_p = 0.3$ , the TF transition density is larger than the prediction of the dynamical spinodal. This proton fraction is of particular interest for neutrino trapped matter for which  $y_p \sim 0.3$ . In this case, a complete equilibrium calculation should be done.

The parametrization GDFM has a very special behavior with an instability region larger than all the other models, for quite symmetric matter. However, for very asymmetric matter, the instability region is smaller than that of other DDH models and is of the order of the NLW models.

Another important conclusion drawn in the present work is the dependence of the pasta phase extension on the isospin asymmetry. For the NLWM, it is seen clearly that the pasta phase extension decreases if the isospin asymmetry decreases. For the density dependent models, a reduction of the proton fraction from 0.5 to 0.3 almost does not affect the pasta phase or may increase it within the CP calculation and the dynamical spinodal approach. Within the dynamical spinodal approach, this behavior is due to the small concavity of the spinodal surface for symmetric matter and the deformation of the spinodal due to the presence of protons, electrons, and the Coulomb field. A smaller fraction of protons contributes with less repulsion and gives a larger instability region. Of course the presence of electrons shields the proton repulsion, and therefore the effect is not so strong as it would be for charged matter. An adequate description of electrons and the Coulomb interaction is important to getting a correct description of the pasta phase extension. In Ref. [3], it was shown that the largest pasta phase extension occurs when the inclusion of the Coulomb field is done in a self-consistent way.

We have checked which parametrizations fulfill the constraints imposed in Ref. [5] for the derivative of the symmetry energy and the transition density and pressure. While the density dependent hadronic models are below the lower limit for the symmetry energy derivative, the NLWM are above the upper limit. However, both NL3 and NL3 $\delta$  together with GDFM fall within the transition pressure/density limits, while TW and DDH $\delta$  have too large transition densities. The GDFM parametrization is the one that satisfies the constraints of Ref. [5] more closely. It seems that the relation between both quantities, the slope of the symmetry energy and the transition density, is not, in fact, model free.

If we had considered the limits on the transition density defined in Ref. [14], i.e.,  $0.25 < P_t < 0.65$  MeV/fm<sup>3</sup>, all models studied here have too small transition pressures except for NL3, which lies just at the lower border, and TW. In Ref. [5] it was shown that a larger slope  $L$  gives rise to a smaller transition density and transition pressure. This feature is seen when models within the same framework are considered, namely, NL3 and NL3 $\delta$ . However, no clear trend is seen among the DDH models. In Ref. [23], it was shown that the slope of the symmetry energy of the NLW models differs from the one of density dependent hadronic models. The parametrizations of Skyrme forces, such as SLy230a, NRAPR, or LNS, which have values of  $L$  at saturation close to the ones of DDH models, also have the transition densities close to those of DDH models and above the limit  $0.065$  fm<sup>-3</sup> imposed in Ref. [5]. This seems to show that a more complete relation between the transition pressure and transition density and the equilibrium isovector properties of asymmetric nuclear matter have to be obtained. This could include constraints on the slope and compressibility of the symmetry energy at subsaturation densities. For instance, the NLW models have positive compressibilities of the symmetry energy at subsaturation densities above  $0.05$  fm<sup>-3</sup>, while the DDH models and the recent Skyrme parametrizations have negative compressibilities. Another point that should be mentioned is that the data obtained from isospin diffusion in heavy-ion reactions correspond to isospin asymmetries that are far from the ones occurring at  $\beta$ -equilibrium matter. For these large asymmetries, we expect that the contribution from terms beyond the parabolic approximation for the isospin dependence of the energy density of nuclear matter becomes important [23].

#### ACKNOWLEDGMENTS

D. P. Menezes acknowledges useful discussions with Dr. J. Piekarewicz. This work was partially supported by CNPq and by FCT (Portugal) under the projects POCI/FP/81923/2007, CERN/FP/83505/2008, and SFRH/BPD/29057/2006.

- [1] D. G. Ravenhall, C. J. Pethick, and J. R. Wilson, *Phys. Rev. Lett.* **50**, 2066 (1983).  
 [2] C. J. Horowitz, M. A. Pérez-García, and J. Piekarewicz, *Phys. Rev. C* **69**, 045804 (2004); C. J. Horowitz, M. A. Pérez-García, D. K. Berry, and J. Piekarewicz, *ibid.* **72**, 035801 (2005).

- [3] T. Maruyama, T. Tatsumi, D. N. Voskresensky, T. Tanigawa, and S. Chiba, *Phys. Rev. C* **72**, 015802 (2005).  
 [4] S. S. Avancini, D. P. Menezes, M. D. Alloy, J. R. Marinelli, M. M. W. Moraes, and C. Providência, *Phys. Rev. C* **78**, 015802 (2008).

- [5] Jun Xu, Lie-Wen Chen, Bao-An Li, and Hong-Ru Ma, arXiv:0807.4477v2 [nucl-th].
- [6] C. J. Pethick and A. Y. Potekhin, Phys. Lett. **B427**, 7 (1998).
- [7] Gentaro Watanabe and Hidetaka Sonoda, arXiv:cond-mat/0502515v2 [cond-mat.soft].
- [8] B. Serot and J. D. Walecka, Adv. Nucl. Phys. **16**, 1 (1986).
- [9] G. A. Lalazissis, J. König, and P. Ring, Phys. Rev. C **55**, 540 (1997).
- [10] K. Sumiyoshi, H. Kuwabara, and H. Toki, Nucl. Phys. **A581**, 725 (1995).
- [11] N. K. Glendenning, *Compact Stars* (Springer-Verlag, New-York, 2000).
- [12] P. Gögelein, E. N. E. van Dalen, C. Fuchs, and H. Mütter, Phys. Rev. C **77**, 025802 (2008).
- [13] E. N. E. van Dalen, C. Fuchs, and A. Faessler, Eur. Phys. J. A **31**, 29 (2007).
- [14] Bennett Link, Richard I. Epstein, and James M. Lattimer, Phys. Rev. Lett. **83**, 3362 (1999).
- [15] B. A. Li, L. W. Chen, and C. M. Ko, Phys. Rep. **464**, 113 (2008).
- [16] S. Typel and H. H. Wolter, Nucl. Phys. **A656**, 331 (1999); Guo Hua, Liu Bo, and M. Di Toro, Phys. Rev. C **62**, 035203 (2000).
- [17] T. Gaitanos, M. Di Toro, S. Typel, V. Baran, C. Fuchs, V. Greco, and H. H. Wolter, Nucl. Phys. **A732**, 24 (2004).
- [18] S. S. Avancini, L. Brito, D. P. Menezes, and C. Providência, Phys. Rev. C **70**, 015203 (2004).
- [19] S. S. Avancini, L. Brito, Ph. Chomaz, D. P. Menezes, and C. Providência, Phys. Rev. C **74**, 024317 (2006).
- [20] S. S. Avancini, J. R. Marinelli, D. P. Menezes, M. M. W. Moraes, and C. Providência, Phys. Rev. C **75**, 055805 (2007); S. S. Avancini, J. R. Marinelli, D. P. Menezes, M. M. Moraes, and A. S. Schneider, *ibid.* **76**, 064318 (2007).
- [21] L. Brito, Ph. Chomaz, D. P. Menezes, and C. Providência, Phys. Rev. C **76**, 044316 (2007).
- [22] M. Dutra, O. Lourenço, A. Delfino, J. S. Sá Martins, C. Providência, S. S. Avancini, and D. P. Menezes, Phys. Rev. C **77**, 035201 (2008).
- [23] C. Ducoin, C. Providência, A. M. Santos, L. Brito, and Ph. Chomaz, Phys. Rev. C **78**, 055801 (2008).
- [24] S. Kubis and M. Kutschera, Phys. Lett. **B399**, 191 (1997).
- [25] B. Liu, V. Greco, V. Baran, M. Colonna, and M. Di Toro, Phys. Rev. C **65**, 045201 (2002).
- [26] C. Fuchs, H. Lenske, and H. H. Wolter, Phys. Rev. C **52**, 3043 (1995); H. Lenske and C. Fuchs, Phys. Lett. **B345**, 355 (1995).
- [27] S. S. Avancini and D. P. Menezes, Phys. Rev. C **74**, 015201 (2006).
- [28] J. M. Lattimer, C. J. Pethick, D. G. Ravenhall, and D. Q. Lamb, Nucl. Phys. **A432**, 646 (1985).
- [29] H. Shen, H. Toki, K. Oyamatsu, and K. Sumiyoshi, Nucl. Phys. **A637**, 435 (1998).
- [30] Y. K. Gambhir, P. Ring, and A. Thimet, Ann. Phys. (NY) **198**, 132 (1990).
- [31] A. Rabhi, C. Providência, and J. da Providência, J. Phys. G **35**, 125201 (2008).
- [32] C. Providência, L. Brito, S. S. Avancini, D. P. Menezes, and Ph. Chomaz, Phys. Rev. C **73**, 025805 (2006); L. Brito, C. Providência, A. M. Santos, S. S. Avancini, D. P. Menezes, and Ph. Chomaz, *ibid.* **74**, 045801 (2006); A. M. Santos, L. Brito, and C. Providência, *ibid.* **77**, 045805 (2008).
- [33] C. Ducoin, K. H. O. Hasnaoui, P. Napolitani, Ph. Chomaz, and F. Gulminelli, Phys. Rev. C **75**, 065805 (2007).
- [34] K. Oyamatsu and K. Iida, Phys. Rev. C **75**, 015801 (2007).